



Exponential improving in the activity of Pt/C nanoparticles towards glycerol electrooxidation by Sb ad-atoms deposition



Gabriella L. Caneppele^{a,1}, Thiago S. Almeida^{a,1}, Cinthia R. Zanata^{a,b}, Érico Teixeira-Neto^c, Pablo S. Fernández^d, Giuseppe A. Camara^b, Cauê A. Martins^{a,*}

^a Faculty of Exact Sciences and Technology, Federal University of Grande Dourados, 79804-970, Dourados, MS, Brazil

^b Chemistry Institute, Federal University of Mato Grosso do Sul, C.P. 549, 79070-900, Campo Grande, MS, Brazil

^c Laboratorio Nacional de Nanotecnologia, CNPEM, C.P. 6192, CEP 13083-970, Campinas, SP, Brazil

^d Institute of Chemistry, Universidade Estadual de Campinas, Cidade Universitária "Zeferino Vaz", Barão Geraldo, CEP 13083-970, Campinas, SP, Brazil

ARTICLE INFO

Article history:

Received 16 March 2016

Received in revised form 24 June 2016

Accepted 28 June 2016

Available online 29 June 2016

ABSTRACT

Tuning the chemical composition of heterogeneous nanocatalysts has emerged as an efficient strategy to improve their electroactivity and selectivity for electrolyzers and fuel cells application. The stability of a catalyst is ascribed as the ability of the nanoparticles (NPs) in maintaining their chemical composition and physical structure during recycles of use. By an electrochemical procedure, here we decorated platinum nanoparticles supported on carbon with different coverage degrees of antimony ad-atom (θ_{Sb}) to investigate glycerol electrooxidation reaction (GEOR). The successful decoration of Pt/C with Sb was monitored by electrochemical and physicochemical characterizations. θ_{Sb} is highly dependent on the upper potential applied. Sb atoms are rapidly leached from Pt surface in potentials greater than 0.7 V in acid solution while they remain stable during several cycles in potentials lower than that. We showed that the current density of GEOR exponentially increases with the increase of Sb coverage, reaching 109 times the pseudo stationary current density of Pt/C for high θ_{Sb} . Furthermore, the ad-atom facilitates the reaction by shifting the onset potential towards lower potentials. We found an improvement of -320 mV in the onset for $\theta_{\text{Sb}} = 0.81$.

© 2016 Elsevier B.V. All rights reserved.

1. Introduction

The identification of nanomaterials that can electrooxidize alcohols through an efficient pathway remains a key challenge for the commercialization of direct alcohol fuel cells (DAFCs). In general, the restricted ability of Pt nanoparticles (NPs) in cleaving C–C bond of small chain alcohols, as ethanol [1], ethylene-glycol [2] and glycerol [3], limits the performance of low-temperature DAFCs. Moreover, the poisoning of active sites of Pt due to the adsorption of partially electrooxidized molecules, compromises the activity of the catalyst. Nonetheless, some compounds produced during incomplete oxidation pathways may have commercially valuable, which is the case of glycerol partial oxidized products on Pt surfaces modified with ad-atoms [4–6].

The production of high-value molecules from glycerol (which is a surplus byproduct of biodiesel fabrication), can be tuned by the chemical composition of the catalyst and the experimental condition, as pH and applied potential [4,6–8]. Despite many efforts, the understanding of how many high active materials act is still scarce [9]. The group of M. T. M. Koper has reported important advances in this field. Kwon et al. showed that Pb, Bi, In, Sn and Sb decorated Pt/C NPs enhance the glycerol electrooxidation reaction (GEOR) [4]. Briefly, these authors found that Pt/C covered with Sb improve GEOR and displace the reaction pathway towards the formation of dihydroxyacetone. In another work, Kwon et al. proposed a Bi-modified Pt catalyst which is 100% selective to the formation of dihydroxyacetone (not considering volatile products) [5].

Regarding the electrochemistry of shape, size and nature (chemical composition) controlled nanoparticles, the group of J. M. Feliu has reported noticeable results [10–12]. Vidal-Iglesias et al. investigated the influence of well-shaped Pt nanoparticles decorated with Sb applied to the electrooxidation of formic acid [10]. They found that Sb-decorated octahedral Pt NPs are the most active materials. Figueiredo et al. showed the electrooxidation of ethanol is sensitive

* Corresponding author.

E-mail addresses: cauealvesmartins@gmail.com, cauemartins@ufgd.edu.br (C.A. Martins).

¹ These authors contributed equally.

to the Sb coverage on Sb-decorated PtRu/C [11]. They found that the activity of the catalysts presents a maximum for coverages around 0.47. The authors showed that direct ethanol fuel cells operating with PtRu/C-Sb as anode displays higher power densities than Pt/C [11].

Among many multimetallic Pt-based catalysts, the results observed for antimony-platinum combinations are encouraging. Hence we decide to test these materials for glycerol. Namely, herein we investigate the influence of the Sb coverage degree on Pt/C NPs towards glycerol electrooxidation through an electrochemical protocol. We have found an exponential augment of the catalytic activity up to $\theta_{\text{Sb}} = 0.81$. Besides, we show that the Sb atoms remain on the Pt surface only at potentials bellow 0.70 V.

2. Methods

2.1. Synthesis of Pt/C nanoparticles

Carbon-supported Pt NPs were prepared using the fast polyol method assisted by micro-waves [13,14]. Briefly, proper amounts of H_2PtCl_6 , poly(acrylic acid salt) (PA, Mw = 2100) and 20 mL of an aqueous solution of ethylene glycol (3 EG:1 H_2O) were sonicated during 5 min followed by the addition of Carbon Vulcan XC72® and sonication for more 20 min. The size and the distribution of NPs were controlled by adjusting the PA/metal ratio to 5.0. The metal load of the Pt/C was set to 40%. The chemical reduction was led in a household microwave oven during 30 s. The aqueous dispersion containing Pt and carbon was washed with deionized water and centrifuged five times to eliminate residues of the synthesis. Finally, the cleaned dispersion was dried in oven under 60 °C for 24 h. After dried, the black powder was used as catalyst.

2.2. Preparation of electrodes and electrochemical measurements

The nanoparticle dispersions, hereafter named inks, were prepared by sonicating (20 min) a mixture of 1 mg of the powder and 1 mL of water. An aliquot of 30 μL of the ink was dropped onto a 0.2 cm^2 glassy carbon electrode (polished to a mirror finish with alumina suspension and rising in ultrasonic bath) to build an electrode with a load of $\sim 40 \mu\text{g cm}^{-2}$. All electrochemical experiments were carried in a three-electrode cell using an oxygen-free 0.1 mol L⁻¹ HClO_4 solution. A glassy carbon rod modified with Pt/C was used as working electrode, a high surface area Pt plate as counter electrode and a reversible hydrogen electrode (RHE) as reference. Prior to prepare the catalyst, we checked the cleanness of the glassy carbon at the same medium at the range of 0.05–1.2 V vs. RHE (no measurement was started without this protocol). We used different potential ranges for each specific case, detailed in due course through the text. The current densities (j) were calculated as a ratio between electrochemical current (i) and electrochemical active surface area (ECSA) of Pt. To calculate the ECSA, we used 210 μC as the charge involved in the desorption of hydrogen per square centimeter of active Pt sites.

2.3. Composition and structure characterization

The Pt/C NPs which were used as base and blank for the whole study involving the coverage degree of Sb were characterized by spectroscopic and microscopic techniques whose experimental details are given below. The identity of Pt/C was investigated by Energy Dispersive X-ray (EDX) detector attached to a scanning electron microscopy JEOL model JSM6380-LV. The X-ray photoelectron microscopy (XPS) was performed with a VSW HA100 electron analyzer in the fixed analyzer transmission mode (FAT) with a pass energy of 44 eV. Al K α radiation was used for excitation (1486.6 eV).

The analysis chamber worked in a vacuum of 10^{-8} mBar. We calibrated the analyzer using Au 4f7/2 line at 84 eV. Pt/C was added and pressed to an In surface to avoid influence of the carbon support. Scofield cross sections [15] were used and the intensities were corrected and the free paths associated with the different kinetic energies of the photoelectrons. We investigated the crystallography of Pt/C by X-ray diffraction (XRD), performed in a Siemens model D5000 powder diffractometer, equipped with a monochromatic Cu K α X-ray source. The data were collected in step sizes of 0.02° between 5° and 90° .

The morphology and size distribution of the Pt/C NPs were characterized by transmission electron microscopy (TEM) and high resolution TEM (HRTEM) by using a CM 200 Philips microscopy operating with a LaB₆ emission gun. The device was equipped with an ultratwin objective and operated at 200 keV. Images were treated using the software Axio Vision SE64 Rel.4.8.

The deposition of Sb atoms on individual Pt nanoparticles was confirmed by the acquisition of compositional maps using a JEOL-JEM 2100F transmission electron microscope available at the Nanotechnology National Laboratory (LNNano) (CNPEM, Campinas, SP). Catalysts were imaged using the high angle annular dark field (HAADF) technique. The X-ray energy dispersive spectrum imaging technique (XEDS-SI) was employed with a Digital Micrograph 1.8 system (Gatan, Inc.) controlling a Thermo-Noran XEDS. The spectrum images (SI) were acquired with a dwell time of 1.0 s/pixel using the drift correction facility at every 100 s. XED spectra were acquired in the 0–20 keV energy range at each pixel. Electron probe sizes of ca. 1.0 nm were obtained operating the JEM 2100F instrument in scanning mode (STEM), allowing enough current density at each sample point for the acquisition of statistically significant X-ray counts for the investigated elements.

3. Results

3.1. Physical characterization of Pt/C

Pt/C NPs decorated with Sb were characterized in terms of electronic properties, crystallinity, morphology and chemical composition. The detailed physical characterization can be seen in Supplementary Materials, Section I. EDX measurement showed the identity of Pt/C (Fig. S1). XPS spectra display the characteristic peaks of Pt and amorphous carbon (Fig. S2). XPS analysis showed that most of the catalyst is in metallic form, containing 20% of oxides. Besides, the metal loading calculated by XPS is 26% metal/carbon (w:w), which is obviously different from the nominal composition (40%). The XPS analysis provides information about the surface composition of the material. The accuracy of the composition compared to the bulk material is high when the NPs are very small. Since the Pt/C NPs have 2.4 ± 0.5 nm of mean diameter, the argument of using XPS analysis does not completely support the huge difference between nominal and real composition. Such difference is entirely ascribed to the aforementioned argument added to the use of weak reducing agent and the extremely fast procedure of synthesis, as published elsewhere [14].

XRD pattern depicts the Pt reflection peaks ascribed to (111), (200), (220) and (311) planes of Pt-type fcc structure (Fig. S3). Moreover, the XRD spectrum reveals a typical reflection peak of (002) planes of carbon support (Fig. S3). The fast polyol method assisted by microwaves yields remarkably well-dispersed NPs over the support, as shows TEM images in Fig. S4. The Pt NPs are mainly spherical and extremely small, with approximately 2.4 ± 0.5 nm of mean diameter. The spherical morphology and the small size result in non-oriented polycrystalline Pt surfaces.

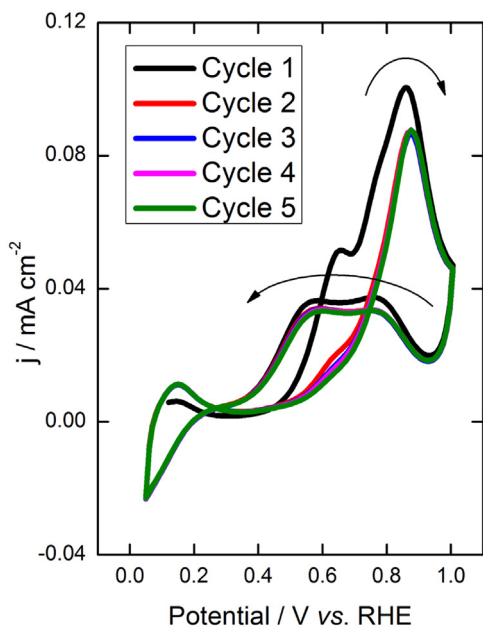


Fig. 1. Electrochemical profile of Pt/C nanoparticles in $0.1 \text{ mol L}^{-1} \text{ HClO}_4 + 0.2 \text{ mol L}^{-1}$ glycerol. Measurements were carried out at 25°C at 0.05 Vs^{-1} .

3.2. Electrochemical measurements

Electrochemical measurements are well-known as *in situ* probe for surface nature and structure [12] while TEM and STM are typical *ex situ* techniques. In this sense, the surface can be characterized by investigating the metal-solution interface through voltammetry. The characteristic electrochemical profile of the carbon supported Pt in $0.1 \text{ mol L}^{-1} \text{ HClO}_4$ is shown in Figs. S5 and S6. Prior to perform any experiments we followed a surface conditioning protocol, which is detailed in Supplementary Materials, Section II. Right after prepared, the Pt/C electrode was immersed in electrolyte solution and cycled ten times between the region of hydrogen under potential deposition (hydrogen UPD) and the region of formation/reduction of surface oxides (Fig. S5). This procedure guarantees the cleaning and conditioning of the surface, providing reliability among the measurements. The decoration procedure and the catalysis measurements only underwent after collecting a typical voltammogram of Pt/C (Figs. S6). The electrooxidation of glycerol on the synthesized Pt/C is shown in the next sub-section.

3.2.1. Glycerol electrooxidation on Pt/C

Glycerol electrooxidation reaction has been thoroughly studied [3,16,17] and some works point out the influence of the structure in an atomic level on the activity of the catalyst [18–20]. Thus, it is paramount to describe the reaction on the NPs used here. All potential cycles show anodic currents during the positive potential scan (forward) and negative potential scan (backward). The first cycle of GEOR is obviously quite different from the second cycle onwards, as shows Fig. 1. The electrochemical profile, under the range of potential used here (0.05 – 1.00 V started at 0.12 V), seems stable from the third cycle onwards. The forward sweep of the first cycle displays a broad region of anodic currents from 0.45 V up to 1.00 V , which is more likely a superimposition of two peaks, located at 0.65 V and 0.85 V . The backward scan depicts a wide plateau of anodic currents, which also can be ascribed as a superimposition of at least two peaks, at 0.75 and 0.55 V . As cycles proceed, the anodic peaks during the backward scans experience less dramatic changes than the peaks from the onward scans.

The difference between the successive cycles has been studied before on both bulk Pt [21] and Pt NPs [14]. Based on previous works, the changes among the cycles are ascribed to a competition between two events: (i) the poisoning of Pt surfaces due to intermediates partially oxidized [21], as we can see by the depletion of the hydrogen UPD region and (ii) the structural surface rearrangements due to the generation of surface defects [19]. The response of bulk polycrystalline Pt (and also this kind of nanoparticles) can be understood as an independent contribution of (110) and extremely disordered (111) and (100) domains [20].

Here we would like to stress the importance of describing the stable electrocatalytic performance of any surface. Otherwise, the response would show the performance of the material only right at the beginning of the experiment, which might not be representative. For instance, the activity obtained from the first cycle is frequently different from that of the stable cycles, which in turn, indeed represents the activity of the material. Thus, we applied the derivative of the voltammetry to obtain the onset potential and peak potential of the first and stable cycles of GEOR [22]. The onset potential shifts from 0.45 V in the first cycle to 0.63 V in the stable cycle. The peak at 0.66 V found in the first cycle is vanished at the stable one while the main peak at 0.86 V remains virtually at the same potential. (As firstly applied to GEOR, the deep interpretation of the dj/dE is found in a comparative study with decorated NPs in Supplementary Materials, Section VI. This section will be cited once again in due course through the text).

After this initial characterization of Pt/C NPs for GEOR, we investigated the influence of the Sb coverage degree for such reaction.

3.3. Electrochemical behavior of Sb-decorated Pt/C in acid medium

There are many methods to produce catalysts for alcohol electrooxidation [6,8,11,14,23–26], in most of them the metallic precursors are mixed and the NPs are formed in the presence of a reducing agent assisted by moderated or high temperatures (or ultrasonic bath). As aforementioned, the SbPt-derived catalysts have been opened up a new class of highly active materials to be used for GEOR, in both direct glycerol fuel cells and electrolyzers. Understanding the influence of the composition of this binary catalyst is imperative to help designing multimetallic nanocatalysts. Thus, it is important to understand the effect of the presence of Sb on Pt/C prior to design SbPt-based materials.

In this sense, we used a potentiodynamic method to produce Sb-decorated Pt/C. As hydrogen does not adsorb onto Sb, this method allows controlling the coverage surface *in situ* by checking the suppression of the hydrogen UPD region [10]. Thus, the Sb coverage (θ_{Sb}) can be accessed by following the changing of area in the hydrogen UPD region (Fig. 3). θ_{Sb} was calculated based on previous work [11], as shows Eq. (1):

$$\theta_{\text{Sb}} = 1 - \theta_{\text{H}} = (q_{\text{H}}^0 - q_{\text{H}}^{\text{Sb}}) / q_{\text{H}}^0 \quad (1)$$

where q_{H}^0 is the charge involved in the hydrogen desorption on Pt/C and q_{H}^{Sb} is the charge involved in the hydrogen desorption on Sb-decorated Pt surface. All Sb coverages were estimated considering 1.0 as a full layer of Sb, that is, the complete suppression of the hydrogen UPD region. The different θ_{Sb} were obtained by changing the number of cycles to which the Pt/C modified glassy carbon was exposed to a solution containing 10^{-5} – $10^{-3} \text{ Sb}_2\text{O}_3 \text{ mol L}^{-1} + 0.1 \text{ mol L}^{-1} \text{ HClO}_4$. Fig. 2 shows that the hydrogen UPD region decreases with the number of cycles, which is evidence that the Pt surface is being covered. Moreover, Pt ($\theta_{\text{Sb}} = 0$) does not show any faradaic current between 0.40 and 0.80 V (Fig. S6), this region presents only capacitive current known as double layer region. On the other hand, the irreversible adsorption of Sb

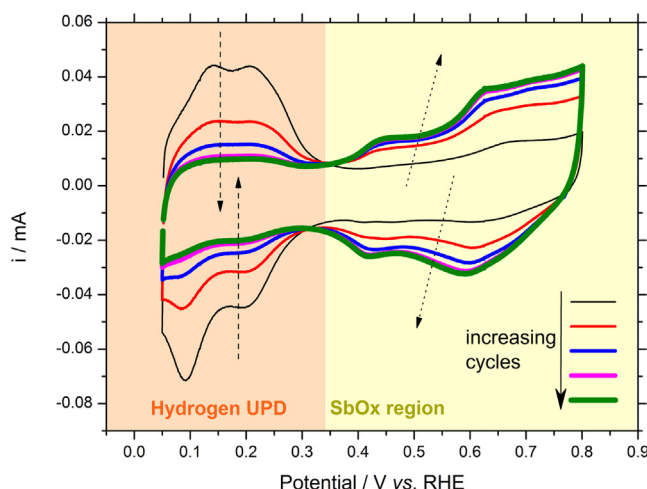


Fig. 2. Successive voltammetric cycles of Pt/C nanoparticles in the presence of 0.003 mol L^{-1} Sb_2O_3 and 0.1 mol L^{-1} HClO_4 between 0.05 and 0.80 V vs. RHE at 0.05 Vs^{-1} during 36 cycles. The two regions show the decreasing of hydrogen UPD and the increasing in the formation/reduction of Sb oxides as a consequence of Sb deposition on Pt.

on Pt sites promotes two redox processes, one at around 0.40 V and other close to 0.60 V (vs. RHE). The detailed decorating procedure can be accessed in Supplementary Materials, Section III.

Vidal-Iglesias et al. used an interesting new method to estimate θ_{Sb} for values close to a monolayer on well-shaped Pt NPs [10]. They found the dependence of the activity reaching coverage degrees greater than 1.0 . In our case, using carbon-supported Pt NPs, we were not able to decorate Pt with θ_{Sb} higher than 0.81 . Fig. S7 (Supplementary Materials, Section III) shows that even though the hydrogen UPD region is totally suppressed in the presence of Sb_2O_3 , the profile of the decorated electrode does not keep that expected θ after being transferred to a cell containing only a HClO_4 solution. This feature is observed even when we cycle the electrode sev-

eral times to a θ virtually greater than 1.0 in Sb_2O_3 . Probably some amount of easily ionized Sb leaves the surface when we slightly wash the electrode before we transfer it to the electrolyte solution. Furthermore, the same work aforementioned showed that a maximum in activity is attained before the full blocking of the active site of Pt surface [10], keeping the synergic effect. Fig. S8 shows the profiles of the Sb-decorated Pt/C NPs.

The deposition of Sb ad-atoms on the surface of Pt/C nanoparticles was demonstrated by elemental mapping using XEDS-SI. The obtained elemental maps (Fig. S9) show the distribution of the measured Sb X-ray over Pt nanoparticles, evidencing the successful decoration by Sb ad-atoms. Besides, since we do not detect an increasing in the NPs mean size, results suggest that the method is reliable to deposit relatively low quantities of Sb.

3.4. Electrochemical stability of Sb-decorated Pt/C in acid medium

It is possible to tune the products of glycerol oxidation by changing the working electrode potential on SbPt [4] and on Pt/C [7]. Some compounds are preferentially yielded only at potentials greater than 1.20 V (vs. RHE) [4]. On the other hand, the electrooxidation of glycerol in potentials greater than 0.60 V (vs. RHE) is not interesting for fuel cells application. Hence, it is crucial to identify the potential stability window of Sb/Pt/C nanocatalysts. In this sense, we performed 40 successive potential cycles using different upper potentials in attempt to follow the stability of the Sb-decorated surface when it experiences distinct applied electric fields. Supplementary Materials, Section IV shows experimental details.

Fig. 3A shows the second cyclic voltammogram for several potential ranges, in which we can follow the changes of the respective profiles. Fig. 3B presents the electrochemical profiles recorded before and after the entire experiment (described in Fig. S10). The profiles after the successive cycles with increasing upper potential completely changed. Namely, the region of formation/reduction of Sb oxides decreases while the hydrogen UPD region increases, indi-

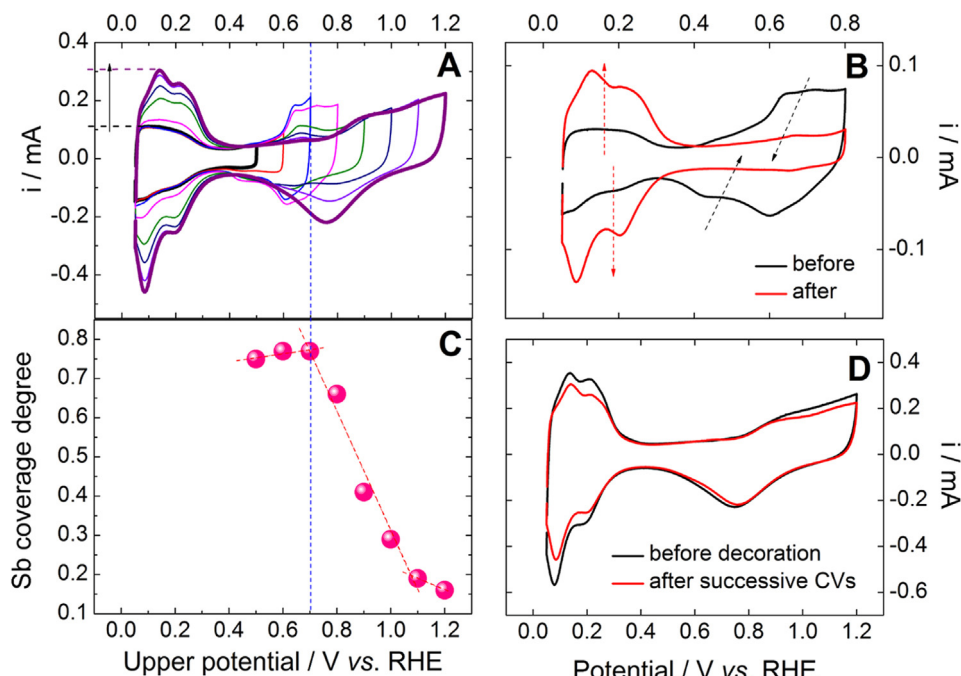


Fig. 3. (a) Second cyclic voltammograms (of 40) of $\theta_{\text{Sb}} = 0.75$ Sb/Pt/C in 0.1 mol L^{-1} HClO_4 at 0.05 Vs^{-1} applying crescent upper potentials (indicated in the Figure). (b) Electrochemical behavior before and after the successive cycles in the different potentials. (c) The variation of Sb coverage degrees with progressive increase potential cycles. (d) Electrochemical profile of Pt/C before the decoration procedure and of $\theta_{\text{Sb}} = 0.75$ Sb/Pt/C catalyst after the successive cycles.

cating leaching of Sb and enrichment of Pt on surface (see Fig. S11 for more details). This phenomenon is not novel. When potentials where molecular oxygen begins to reduce are reached, the multimetallic catalyst leaches the less noble metal from the surface, as showed by Cui et al. for PtNi [28]. Thus, it is pivotal to find the potential domain where a given catalyst is able to keep its activity.

In this sense, we followed the θ_{Sb} at these progressive increasing potentials (Fig. 3C). θ_{Sb} is constant ($\theta_{\text{Sb}} \sim 0.75$) while the upper potentials were kept lower than 0.7 V, as shows the fitted line from 0.5 to 0.7 V in Fig. 3C. This feature is evidenced by the indiscernible changes in the hydrogen UPD region (upper potentials of 0.5, 0.6 and 0.7 V in Fig. 3A). However, successive cycles applying potentials greater than 0.7 V result in a sudden decrease of θ_{Sb} , as shows the fitted line from 0.7 to 1.1 V (Fig. 3C). Therefore, Sb/Pt/C-based catalysts are interesting for fuel cells and electrolyzers application, as long as the electrochemical potential is kept lower than 0.7 V to avoid loss of Sb with consequent changes in the characteristics of the catalyst.

Sb almost completely leaches from Pt surface when high upper potentials are reached, consequently the hydrogen UPD region increases and the electrochemical behavior become similar to bare Pt/C in acid medium before the decoration procedure (Fig. 3D). The small difference of these profiles can be ascribed to the cleaning and degradation processes experimented by the NPs during the potential cycling [27]. The region of formation/reduction of surface oxides on Pt is better defined on the cycled Pt NPs, suggesting surface cleaning. Additionally, the H_{UPD} region is slightly smaller due to some agglomeration/degradation processes [27]. However, we cannot ignore the possibility of Sb traces remain on the surface of Pt sites. Fig. S12 shows a statistic analysis of the average variation of Sb coverage degrees and the features are commented in Supplementary Materials, Section IV.

After being established the potential window in which Sb remains stable over the surface, the next section is devoted to the influence of the Sb coverage degree on the glycerol electrooxidation.

3.5. Glycerol electrooxidation on Sb-decorated Pt/C nanoparticles

We evaluated the glycerol electrooxidation on Pt/C before and after the ad-atom decoration. Although the safest way of maintaining the nature of the catalyst would be keeping the upper potential minor than 0.7 V, here we studied the GEOR in the range of potential 0.05–0.80 V in attempt to follow the decrease of the main anodic peak, which is well-defined only at this potential range. Fig. 4 shows the first and the stable positive potential sweep taken from five successive cycles (detailed in Fig. S13 and discussed in Supplementary Materials, Section V). We denote stable (or pseudo stationary-state) cycle to the fifth one. Here we point out that the θ_{Sb} decreases ~5% from the first to the fifth cycle, taken into account the decrease in coverage degree of a $\theta_{\text{Sb}} = 0.75$ decorated Pt/C NPs cycled up to 0.8 V.

The addition of Sb on Pt/C leads to an increase of its performance for GEOR (Fig. 4). These results are in line with those of Figueiredo et al. [11], who investigated the ethanol electrooxidation on Sb-decorated Pt/C and PtRu/C catalysts and with Vidal-Iglesias et al. [10], who studied formic acid electrooxidation on Sb-decorated well-shaped and non-supported Pt NPs. The Sb/Pt/C catalyst with $\theta_{\text{Sb}} = 0.30$ does not show any significant improvement in the catalysis compared to bare Pt, which suggests that isolated Sb isles formed on low covered surfaces do not drive the reaction towards a catalytic pathway. This result suggests that the synergic effect on the neighborhood of both Pt and Sb improves the catalytic reaction and this effect increases as θ_{Sb} grows.

On the other hand, high θ_{Sb} impact the GEOR in terms of current density and onset potential. At 0.5 V, the current density of

$\theta_{\text{Sb}} = 0.75$ Sb/Pt/C is 6.4 times higher than the non-decorated catalyst. Interestingly, for the first cycles, the performance of $\theta_{\text{Sb}} = 0.75$ and $\theta_{\text{Sb}} = 0.81$ surfaces are virtually the same up to 0.54 V, where the slope of the voltammogram starts diminishing for $\theta_{\text{Sb}} = 0.75$, while keeps growing until 0.56 V for $\theta_{\text{Sb}} = 0.81$. The presence of Sb anticipates the onset potential, indicating that the ad-atom facilitates the reaction. The analysis of the derivative voltammetry reveals that the GEOR starts at 0.31 V on $\theta_{\text{Sb}} = 0.81$ Sb/Pt/C, which represents a shift of 320 mV towards lower potentials, as shows Fig. S14 (detailed in Supplementary Materials, Section VI).

In general, the currents decrease from the first to the stable cycle (detailed in Supplementary Materials, Section V). The most important feature here is that more covered are the Pt/C NPs, the slighter is the decreasing of current (Fig. 4) from the first to the stable profile. Non-decorated Pt/C and $\theta_{\text{Sb}} = 0.11$ Sb/Pt/C show the lowest current densities during the first and stable cycles, while higher coverage degrees hold higher currents in the stable cycle. This supposition is proved by looking at the performance of the first and stables cycles of $\theta_{\text{Sb}} = 0.75$ and $\theta_{\text{Sb}} = 0.81$ catalysts (Fig. 4a and b, respectively). The surface containing $\theta_{\text{Sb}} = 0.75$ suffers a more intense loss of activity than $\theta_{\text{Sb}} = 0.81$. Fig. 4b shows that at 0.5 V the current density of $\theta_{\text{Sb}} = 0.81$ Sb/Pt/C is 41.7 times higher than the non-decorated catalyst, which is an outstanding improvement of activity.

Regarding the influence of the surface coverage degree on its ability of maintaining activity, we followed the current density of five cycles of GEOR on $\theta_{\text{Sb}} = 0.0$ (Fig. 5a) and $\theta_{\text{Sb}} = 0.81$ (Fig. 5b), and compare them in Fig. 5c. Except for the first values, the current density at 0.6 V ($j(0.6\text{ V})$) tends to be stable and the slope of this curves diminishes for higher coverages, corroborating the evidence aforementioned that the presence of great amounts of Sb stabilizes the electrochemical response of the catalyst in elevated magnitudes (fitted dashed lines in Fig. 5c).

The activity of the nanocatalysts in conditions closer to those experienced in fuel cells was also evaluated by following the pseudo-stationary current densities obtained through chronoamperometries. The catalysts were polarized at 0.12 V and the working electrode potential was stepped to 0.5 V for 1800s in the presence of glycerol and the supporting electrolyte, as shows Fig. 6. The pseudo stationary current densities increase exponentially with the Sb coverage from $\theta_{\text{Sb}} 0.00\text{--}0.81$ (inset of Fig. 6). The potentiostatic experiments are in line with the potentiodynamics, showing that covering Pt/C NPs with Sb increase the kinetics of GEOR. Pseudostationary j for $\theta_{\text{Sb}} = 0.81$ Sb/Pt/C is ~109 times more intense than that of Pt/C.

Leiva et al. followed the current density produced from formic acid electrooxidation on Sb-covered Pt(100) surfaces, comparing theoretical and experimental data [29]. These authors found that the current density increases exponentially with θ_{Sb} until an inflection region at approximately $\theta_{\text{Sb}} = 0.80$ and suddenly decreases for higher coverings [29]. The features of θ_{Sb} on Pt seem similar for formic acid and glycerol electrooxidation in terms of current density profile (j vs. θ_{Sb}). The inset of Fig. 6 shows an exponentially improvement in the activity of the catalyst toward GEOR with the increase of Sb ad-atom covering Pt/C NPs.

In summary, the electrochemical investigation proves that Sb-decorated Pt/C NPs facilitate the glycerol oxidation reaction, anticipating the onset potential and augmenting the current density in all the potential domains (with an exponential increase at 0.5 V in pseudostationary conditions). Kwon et al. showed a massive production of dihydroxyacetone on Sb-decorated Pt/C NPs starting at the reaction onset potential [4]. On the other hand, we previously showed [19] for several Pt surfaces that carbonyl containing compounds started to be formed at high potentials, only after some CO removal. A systematic comparison using spectroelectrochemical and analytic techniques will help to deciphering the real effect of Sb, but our results suggest that the ad-atoms hinder the GLOH dis-

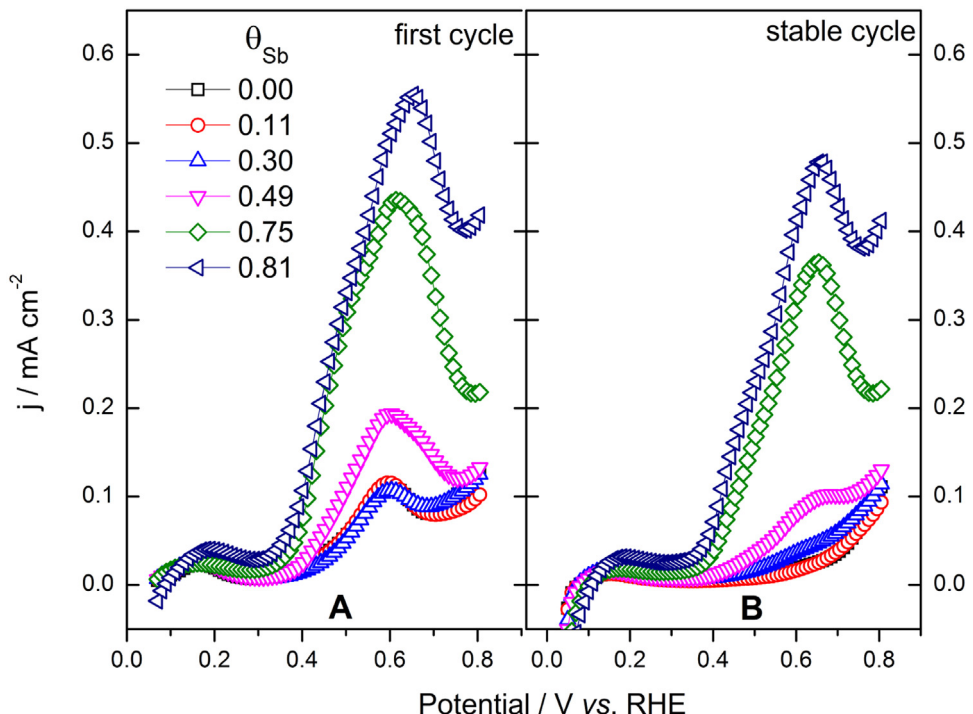


Fig. 4. (a) First and (b) fifth cyclic voltammograms in $0.1 \text{ mol L}^{-1} \text{ HClO}_4 + 0.2 \text{ mol L}^{-1}$ glycerol at 0.05 V s^{-1} . Both series show an increasing of the catalytic activity when θ_{Sb} is bigger than 0.3.

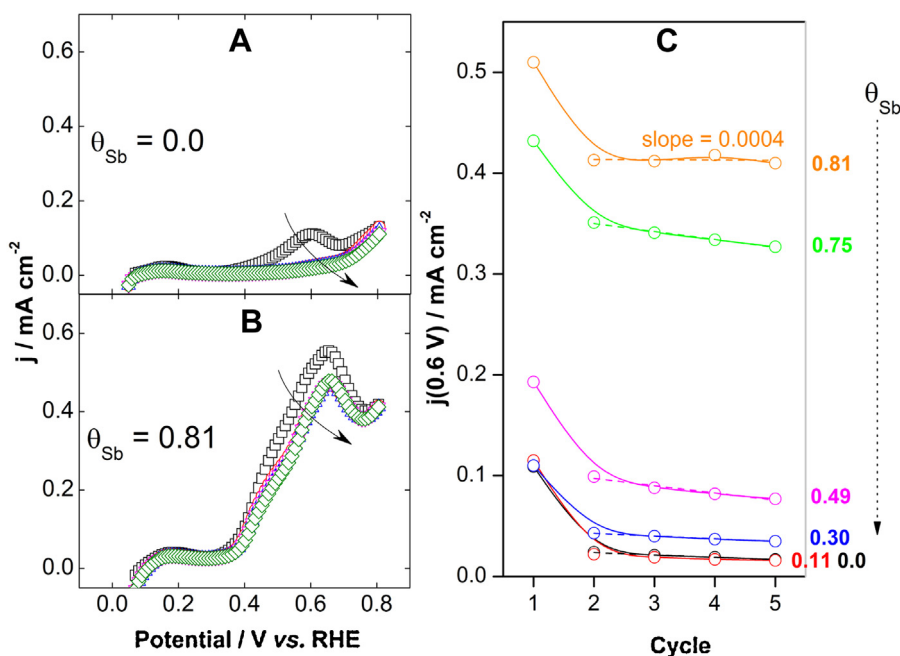


Fig. 5. Five consecutive positive potential going scan of (a) $\theta_{\text{Sb}} = 0.0$ and (b) $\theta_{\text{Sb}} = 0.81 \text{ Sb/Pt/C}$ in $0.1 \text{ mol L}^{-1} \text{ HClO}_4 + 0.2 \text{ mol L}^{-1}$ glycerol at 0.05 V s^{-1} . (c) Current densities at 0.6 V ($j(0.6 \text{ V})$) for the different covered surfaces as a function of cycles. The dashed curves indicate a linear fit of $j(0.6 \text{ V})$ values from second to fifth cycle. θ_{Sb} are indicated in the Figure.

sociative adsorption, preventing the catalyst from being poisoned by GIOH partially oxidized products. This fact permits the GIOH oxidation to carbonyl containing compounds (mainly dihydroxyacetone) at lower potentials. Thus, the reaction onset on Pt surfaces is connected to CO oxidation to CO_2 whereas in the modified surfaces is mainly connected to the selective oxidation of the secondary carbon of GIOH to produce dihydroxyacetone. Furthermore, we found that potentials from 0.5 to 0.7 V represent an electrochemically safe

scenario to operate fuel cells and electrolyzers using Sb/Pt/C catalysts as anode. Potentials greater than 0.7 V rapidly leaches Sb from Pt surfaces, resulting in decrease of activity.

4. Conclusion

The electrochemical decoration procedure allows controlling the reversible deposition of Sb ad-atom on Pt surfaces and the

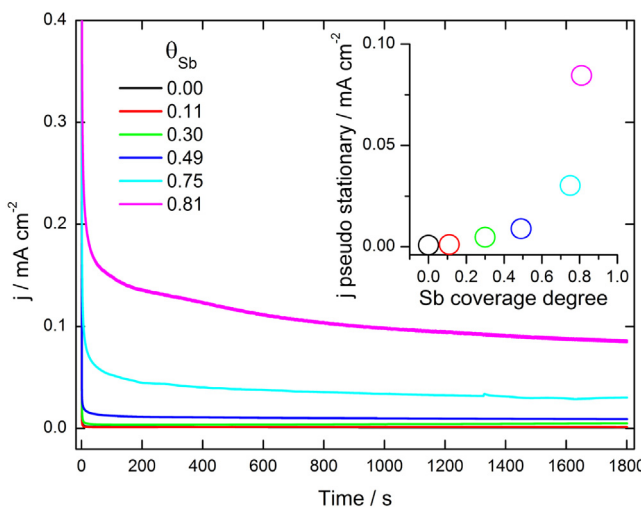


Fig. 6. Chronoamperograms after application of a potential step from 0.12 V to 0.5 V in 0.1 mol L⁻¹ HClO₄ + 0.2 mol L⁻¹ glycerol. Inset shows the pseudo stationary current density for glycerol electrooxidation taken from current-time curves after 1800s of polarization at 0.5 V, plotted as a function of the Sb coverage degree on Pt/C.

investigation of their activities accordingly. The ability of the Sb-decorated Pt/C NPs in keeping their coverage degree (θ_{Sb}) is highly dependent on the potential domain. We found that 0.7 V is the limiting working potential for Sb/Pt/C in acid media. A linear decrease in θ_{Sb} is observed in function of potentials bigger than the limiting one.

Sb/Pt/C NPs are highly electroactive for glycerol electrooxidation reaction (GEOR) in acid media. Potentiodynamic experiments revealed that the current density only increase significantly for coverage greater than $\theta_{Sb} = 0.30$. Thus, isolated isles of Sb on Pt seem to have no catalytic effect on the reaction. High θ_{Sb} produces high currents and shifts the onset potential toward lower potentials. $\theta_{Sb} = 0.81$ Sb/Pt/C displaces –320 mV the onset potential compared to Pt/C.

Potentiostatic experiments show that pseudostationary current densities rise exponentially with the increasing of θ_{Sb} . The remarkable activity reaches 109 times the values found for non-decorated Pt/C.

Therefore, our results show that Sb/Pt/C NPs display an outstanding activity towards GEOR. However, one must assure that this catalyst is used below the limiting working potential found here to avoid loss of stability of electrolyzers and fuel cells operating with Sb/Pt/C as anode.

Author contributions

The manuscript was written through contributions of all authors. All authors have given approval to the final version of the manuscript.

Acknowledgments

The authors acknowledge financial assistance from CNPq (Grant # 454516/2014-2), FUNDECT (Grant # 026/2015), CAPES and FINEP. Authors thank LNNano-CNPEM (Campinas, Brazil) for the use of the TEM facility.

Appendix A. Supplementary data

Supplementary data associated with this article can be found, in the online version, at <http://dx.doi.org/10.1016/j.apcatb.2016.06.072>.

References

- [1] M. Li, D.A. Cullen, K. Sasaki, N.S. Marinkovic, K. More, R.R. Adzic, *J. Am. Chem. Soc.* 135 (2013) 132–141.
- [2] P. Bi, W. Hong, C. Shang, J. Wang, E. Wang, *RSC Adv.* 6 (2016) 12486–12490.
- [3] A. Zalineeva, A. Serov, M. Padilla, U. Martinez, K. Artyushkova, S. Baranton, C. Coutanceau, P.B. Atanassov, *J. Am. Chem. Soc.* 136 (2014) 3937–3945.
- [4] Y. Kwon, T.J.P. Hersbach, M.T.M. Koper, *Top. Catal.* 57 (2014) 1272–1276.
- [5] Y. Kwon, Y. Birdja, I. Spanos, P. Rodriguez, M.T.M. Koper, *ACS Catal.* 2 (2012) 759–764.
- [6] Y. Holade, C. Morais, K. Servat, T.W. Napporn, K.B. Kokoh, *ACS Catal.* 3 (2013) 2403–2411.
- [7] H.J. Kim, J. Lee, S.K. Green, G.W. Huber, W.B. Kim, *ChemSusChem* 7 (2014) 1051–1054.
- [8] T.P. Scachetti, A.C.D. Angelo, *Electrocatalysis* 6 (2015) 472–480.
- [9] P.C.K. Vesborg, T.F. Jaramillo, *RSC Adv.* 2 (2012) 7933–7947.
- [10] F.J. Vidal-Iglesias, A. López-Cudero, J. Solla-Gullón, J.M. Feliu, *Angew. Chem.* 52 (2013) 964–967.
- [11] M.C. Figueiredo, O. Sorsa, R.M. Arán-Ais, N. Doan, J.M. Feliu, T. Kallio, *J. Catal.* 329 (2015) 69–77.
- [12] F.J. Vidal-Iglesias, R.M. Arán-Ais, J. Solla-Gullón, E. Herrero, J.M. Feliu, *ACS Catal.* 2 (2012) 901–910.
- [13] V. Armendáriz, C.A. Martins, H.E. Troiani, L.C.S. de Oliveira, J.M. Stropa, G.A. Camara, M.E. Martins, P.S. Fernández, *Electrocatalysis* 5 (2014) 279–287.
- [14] C.R. Zanata, P.S. Fernández, H.E. Troiani, A.L. Soldati, R. Landers, G.A. Camara, A.E. Carvalho, C.A. Martins, *Appl. Catal. B: Environ.* 181 (2016) 445–455.
- [15] J.H. Scofield, *J. Electron Spectrosc.* 8 (1976) 129–137.
- [16] A.C. Garcia, J. Caliman, E.B. Ferreira, G. Tremiliosi-Filho, J.J. Linares, *ChemElectroChem* 2 (2015) 1036–1041.
- [17] P.S. Fernández, M.E. Martins, C.A. Martins, G.A. Camara, *Electrochim. Commun.* 15 (2012) 14–17.
- [18] J.F. Gomes, F.B.C. de Paula, L.H.S. Gasparotto, G. Tremiliosi-Filho, *Electrochim. Acta* 76 (2012) 88–93.
- [19] P.S. Fernández, J.F. Gomes, C.A. Angelucci, P. Tereshchuk, C.A. Martins, G.A. Camara, M.E. Martins, J.L.F. Da Silva, G. Tremiliosi-Filho, *ACS Catal.* 5 (2015) 4227–4236.
- [20] P.S. Fernández, C.A. Martins, C.A. Angelucci, J.F. Gomes, G.A. Camara, M.E. Martins, G. Tremiliosi-Filho, *ChemElectroChem* 2 (2015) 263–268.
- [21] J.F. Gomes, C.A. Martins, M.J. Giz, G. Tremiliosi-Filho, G.A. Camara, *J. Catal.* 301 (2013) 154–161.
- [22] A. Murthy, A. Manthiram, *J. Phys. Chem. C* 116 (2012) 3827–3832.
- [23] H. Wang, L. Thia, N. Li, X. Ge, Z. Liu, X. Wang, *ACS Catal.* 5 (2015) 3174–3180.
- [24] J. Zheng, D.A. Cullen, R.V. Forest, J.A. Wittkopf, Z. Zhuang, W. Sheng, J.G. Chen, Y. Yan, *ACS Catal.* 5 (2015) 1468–1474.
- [25] A. Zalineeva, S. Baranton, C. Coutanceau, *Electrochim. Acta* 176 (2015) 705–717.
- [26] Y. Zuo, L. Wu, K. Cai, T. Li, W. Yin, D. Li, N. Li, J. Liu, H. Han, *ACS Appl. Mater. Interfaces* 7 (2015) 17725–17730.
- [27] P.S. Fernández, D.S. Ferreira, C.A. Martins, H.H. Troiani, G.A. Camara, M.E. Martins, *Electrochim. Acta* 98 (2013) 25–31.
- [28] C. Cui, L. Gan, M. Heggen, S. Rudi, P. Strasser, *Nat. Mater.* 12 (2013) 765–771.
- [29] E. Leiva, T. Iwasita, E. Herrero, J.M. Feliu, *Langmuir* 13 (1997) 6287–6293.